Supporting Information

Enhancing Conductance in Single-Molecule Junctions through Nitrogen Bridge-Mediated *p*-π Conjugation

Yin Zhao,[a] Wenlong Liu,[a] Yunpeng Li,[a] Rui Wang,[a] Jiawei Yang,[a] Hongxiang Li[a]*

[a.] Key Laboratory for Advanced Materials and Joint International Research Laboratory of Precision Chemistry and Molecular Engineering, Feringa Nobel Prize Scientist Joint Research Center, Frontiers Science Center for Materiobiology and Dynamic Chemistry, Institute of Fine Chemicals, School of Chemistry and Molecular Engineering, East China University of Science and Technology, Shanghai 200237

E-mail: lihongxiang@ecust.edu.cn (H. Li)

Table of Contents

1. General Information

All reactions were carried out under nitrogen atmosphere and anhydrous conditions unless otherwise indicated. Unless otherwise noted, all catalytic reactions were run in dried glassware. The commercial reagents were purchased from Bidepharm, 9dingchem, Adamas-beta China and were used as received. Reactions were monitored by thin-layer chromatography (TLC) carried out on 0.20 mm silica gel plates using UV light as the visualizing agent. All new compounds were characterized by means of ^{1}H NMR, ^{13}C NMR, and HR-MS. NMR spectra were recorded using a Bruker AVANCE III 400 MHz spectrometer. High-resolution mass spectra (HRMS) were recorded on a Waters Xevo G2 TOF MS (EI).

2. Experimental Section

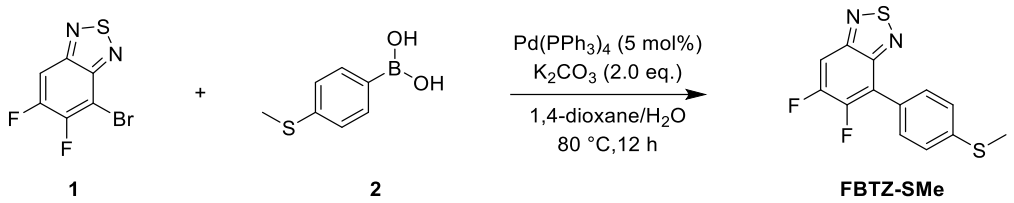

Scheme S1. The synthesis of **FBTZ-SMe**

FBTZ-SMe was synthesized following the reported procedures[1] with minor modifications. To a 100 mL schlenk tube was charged with 4-bromo-5,6-difluorobenzo[c][1,2,5]thiadiazole (**1**, 251 mg, 1.0 mmol), 4-(methylthio)phenylboronic acid (**2**, 202 mg, 1.2 mmol), K_2CO_3 (277 mg, 2.0 mmol) and $Pd(PPh_3)_4$ (58 mg, 0.05 mmol), then the schlenk tube was degassed and backfilled with argon 3 times. The degassed 1,4-dioxane (8 mL) and H_2O (2 mL) were added with syringe, the mixture was allowed heated to 80 ℃ overnight, the reaction mixture was cooled to room temperature and diluted with ethyl acetate, washed with brine and water, dried over Na_2SO_4, filtered and concentrated. The residue was purified with silica gel chromatography using PE/EA=30:1 as eluent to provide product **FBTZ-SMe** as yellow solid (212 mg, yield: 72.1%); ^{1}H NMR (400 MHz, $CDCl_3$) δ 7.74 – 7.71 (m, 3H), 7.42 (d, J = 8.4 Hz, 2H), 2.56 (s, 3H). ^{19}F NMR (376 MHz, $CDCl_3$): δ -127.0 (d, J = 18.8 Hz), -134.1 (d, J = 18.8 Hz). HRMS(EI): m/z calcd. for $C_{13}H_8F_2N_2S_2^+$ $[M]^+$: 294.0097; Found: 294.0099.

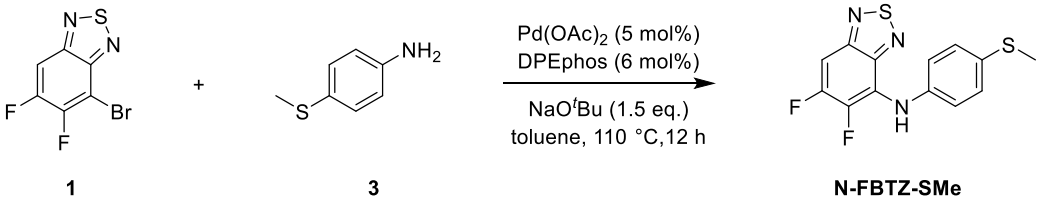

Scheme S2. The synthesis of **N-FBTZ-SMe**

N-FBTZ-SMe was synthesized following the reported procedures[2] with minor modifications. To a 100 mL schlenk tube was charged with 4-bromo-5,6-difluorobenzo[c][1,2,5]thiadiazole (**1**, 251 mg, 1.0 mmol), 4-(methylthio)aniline (**3**, 167 mg, 1.2 mmol), NaO^{t}Bu (144 mg, 1.5 mmol), DPEphos (32 mg, 0.06 mmol) and $Pd(OAc)_2$ (12 mg, 0.05 mmol), then the schlenk tube was degassed and backfilled with argon 3 times. The degassed toluene (10 mL) were added with syringe, the mixture was allowed heated to 110 ℃ overnight, the reaction mixture was cooled to room temperature and diluted with ethyl acetate, washed with brine and water, dried over Na_2SO_4, filtered and concentrated. The residue was purified with silica gel chromatography using PE/EA=20:1 as eluent to provide product **N-FBTZ-SMe** as yellow solid (200 mg, yield: 68.1%); ^{1}H NMR (400 MHz, $CDCl_3$) δ 7.24 – 7.21 (m, 3H), 6.96 (d, J = 8.8 Hz, 2H), 6.68 (s, 1H), 2.45 (s, 3H). ^{19}F NMR (376 MHz, $CDCl_3$): δ -126.1 (d, J = 18.8 Hz), -141.8 (d, J = 18.8 Hz). HRMS(EI): m/z calcd. for $C_{13}H_9F_2N_3S_2^+$ $[M]^+$: 309.0206; Found: 309.0207.

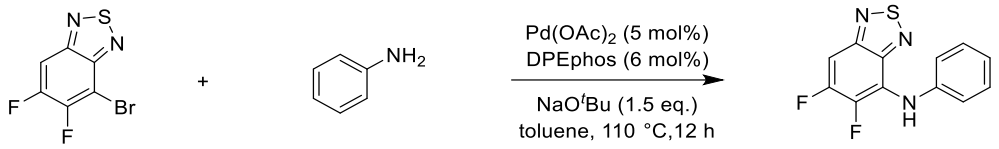

Scheme S3. The synthesis of **N-FBTZ**

N-FBTZ was synthesized following the reported procedures[2] with minor modifications. To a 100 mL schlenk tube was charged with 4-bromo-5,6-difluorobenzo[c][1,2,5]thiadiazole (**1**, 251 mg, 1.0 mmol), aniline (**4**, 112 mg, 1.2 mmol), NaO^{t}Bu (144 mg, 1.5 mmol), DPEphos (32 mg, 0.06 mmol) and $Pd(OAc)_2$ (12 mg, 0.05 mmol), then the schlenk tube was degassed and backfilled with argon 3 times. The degassed toluene (10 mL) were added with syringe, the mixture was allowed heated to 110 ℃ overnight, the reaction mixture was cooled to room temperature and diluted with ethyl acetate, washed with brine and water, dried over Na_2SO_4, filtered and concentrated. The residue was purified with silica gel chromatography using PE/EA=20:1 as eluent to provide product **N-FBTZ** as yellow solid (191 mg, yield: 72.3%); ^{1}H NMR (400 MHz, $CDCl_3$) δ 7.35 – 7.26 (m, 3H), 7.10 – 7.05 (m, 3H), 6.75 (s, 1H). ^{19}F NMR (376 MHz, $CDCl_3$): δ -126.1 (d, J = 15.0 Hz), -141.2 (d, J = 15.0 Hz). HRMS(EI): *m/z* calcd. for $C_{12}H_7F_2N_3S^+$ $[M]^+$: 263.0329; Found: 263.0325.

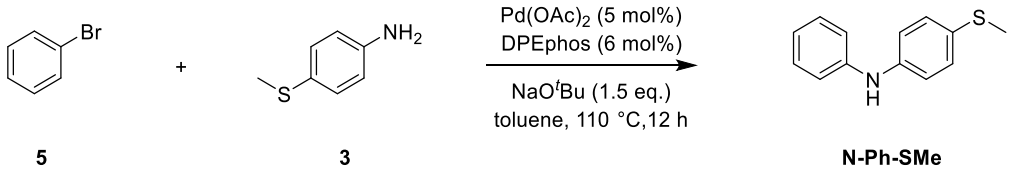

Scheme S4. The synthesis of **N-Ph-SMe**

To a 100 mL schlenk tube was charged with bromobenzene (**5**, 157 mg, 1.0 mmol), 4-(methylthio)aniline (**3**, 167 mg, 1.2 mmol), NaO^{t}Bu (144 mg, 1.5 mmol), DPEphos (32 mg, 0.06 mmol) and $Pd(OAc)_2$ (12 mg, 0.05 mmol), then the schlenk tube was degassed and backfilled with argon 3 times. The degassed toluene (10 mL) were added with syringe, the mixture was allowed heated to 110 ℃ overnight, the reaction mixture was cooled to room temperature and diluted with ethyl acetate, washed with brine and water, dried over Na_2SO_4, filtered and concentrated. The residue was purified with silica gel chromatography using PE/EA=30:1 as eluent to provide product **N-Ph-SMe** as white solid (162 mg, yield: 75.1%); ^{1}H NMR (400 MHz, $CDCl_3$) δ 7.26 – 7.20 (m, 4H), 7.02 (d, J = 8.4 Hz, 3H), 6.98 (s, 1H), 6.91 (t, J = 7.6 Hz, 1H), 5.67 (s, 1H), 2.44 (s, 3H). ^{13}C NMR (101 MHz, $CDCl_3$) δ 143.1, 141.5, 130.0, 129.5, 129.2, 121.2, 118.7, 117.9, 18.0.

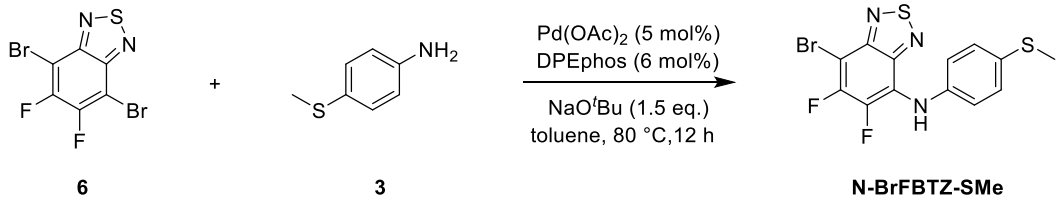

Scheme S5. The synthesis of **N-BrFBTZ-SMe**

N-BrFBTZ-SMe was synthesized following the reported procedures[2] with minor modifications. To a 100 mL schlenk tube was charged with 4,7-dibromo-5,6-difluorobenzo[c][1,2,5]thiadiazole (**6**, 330 mg, 1.0 mmol), 4-(methylthio)aniline (**3**, 140 mg, 1.0 mmol), NaO^{t}Bu (144 mg, 1.5 mmol), DPEphos (32 mg, 0.06 mmol) and $Pd(OAc)_2$ (12 mg, 0.05 mmol), then the schlenk tube was degassed and backfilled with argon 3 times. The

degassed toluene (10 mL) were added with syringe, the mixture was allowed heated to 80 ℃ overnight, the reaction mixture was cooled to room temperature and diluted with ethyl acetate, washed with brine and water, dried over Na_2SO_4, filtered and concentrated. The residue was purified with silica gel chromatography using PE/EA=20:1 as eluent to provide product **N-BrFBTZ-SMe** as orange solid (156 mg, yield: 40.1%); ^{1}H NMR (400 MHz, $CDCl_3$) δ 7.30 – 7.27 (m, 2H), 7.03 (d, *J* = 8.8, 1H), 7.02 (d, *J* = 8.8, 1H), 6.73 (s, 1H), 2.50 (s, 3H). ^{19}F NMR (376 MHz, $CDCl_3$): δ -119.3 (d, *J* = 18.8 Hz), -139.9 (d, *J* = 18.8 Hz). HRMS(EI): *m*/*z* calcd. for $C_{13}H_8BrF_2N_3S_2^+$ $[M]^+$: 386.9311; Found: 386.9311.

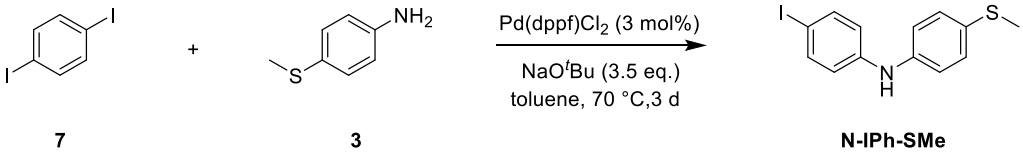

7 **3** **N-IPh-SMe**

Scheme S6. The synthesis of **N-IPh-SMe**

N-IPh-SMe was synthesized following the reported procedures[3] with minor modifications. To a 100 mL schlenk tube was charged with 1,4-diiodobenzene (**7**, 990 mg, 3.0 mmol), 4-(methylthio)aniline (**3**, 140 mg, 1.0 mmol), NaO^{t}Bu (336 mg, 3.5 mmol) and Pd(dppf)Cl_2 (22 mg, 0.03 mmol), then the schlenk tube was degassed and backfilled with argon 3 times. The degassed toluene (10 mL) were added with syringe, the mixture was allowed heated to 70 ℃, the reaction mixture was cooled to room temperature and diluted with ethyl acetate, washed with brine and water, dried over Na_2SO_4, filtered and concentrated. The residue was purified with silica gel chromatography using PE/EA=30:1 as eluent to provide product **N-IPh-SMe** as yellow solid (162 mg, yield: 47.6%); ^{1}H NMR (400 MHz, $CDCl_3$) δ 7.43 (d, *J* = 8.0 Hz, 2H), 7.16 (d, *J* = 8.4 Hz, 2H), 6.92 (d, *J* = 8.4 Hz, 2H), 6.71 (d, *J* = 8.0 Hz, 2H), 5.57 (s, 1H), 2.38 (s, 3H). ^{13}C NMR (101 MHz, $CDCl_3$) δ 143.2, 140.3, 138.2, 130.4, 129.7, 119.5, 119.3, 82.3, 17.7. HRMS(EI): *m*/*z* calcd. for $C_{13}H_{12}INS^+$ $[M]^+$: 340.9735; Found: 340.9733.

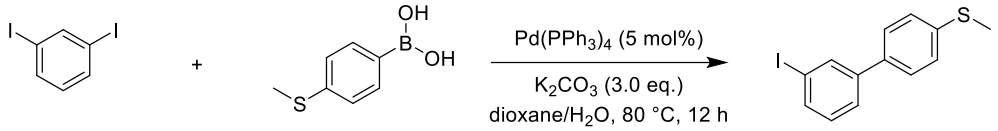

8 **2** **mIPh-SMe**

Scheme S7. The synthesis of **mIPh-SMe**

To a 100 mL schlenk tube was charged with 1,3-diiodobenzene (**8**, 990 mg, 3.0 mmol), 4-(methylthio)phenylboronic acid (**2**, 169 mg, 1.0 mmol), K_2CO_3 (415 mg, 3.0 mmol) and $Pd(PPh_3)_4$ (58 mg, 0.05 mmol), then the schlenk tube was degassed and backfilled with argon 3 times. The degassed 1,4-dioxane (8 mL) and H_2O (2 mL) were added with syringe, the mixture was allowed heated to 80 ℃ overnight, the reaction mixture was cooled to room temperature and diluted with ethyl acetate, washed with brine and water, dried over Na_2SO_4, filtered and concentrated. The residue was purified with silica gel chromatography using PE/EA=30:1 as eluent to provide product **mIPh-SMe** as white solid (150 mg, yield: 47.2%); ^{1}H NMR (400 MHz, $CDCl_3$) δ 7.92 (s, 1H), 7.66 (d, *J* = 8.0 Hz, 1H), 7.52 (d, *J* = 8.0 Hz, 1H), 7.47 (d, *J* = 8.4 Hz, 2H), 7.32 (d, *J* = 8.4 Hz, 2H), 7.16 (t, *J* = 8.0 Hz, 1H), 2.52 (s, 3H). ^{13}C NMR (101 MHz, $CDCl_3$) δ 142.9, 138.6, 136.4, 136.2, 135.9, 130.6, 127.5, 126.9, 126.2, 95.0, 15.9.

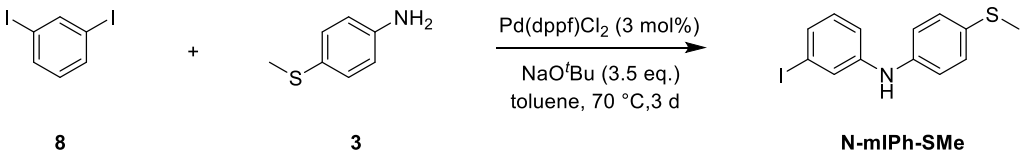

8 **3** **N-mIPh-SMe**

Scheme S8. The synthesis of **N-mIPh-SMe**

N-mIPh-SMe was synthesized following the reported procedures[3] with minor modifications. To a 100 mL schlenk tube was charged with 1,3-diiodobenzene (**8**, 990 mg, 3.0 mmol), 4-(methylthio)aniline (**3**, 140 mg, 1.0 mmol), NaO^{t}Bu (336 mg, 3.5 mmol) and Pd(dppf)Cl_2 (22 mg, 0.03 mmol), then the schlenk tube was degassed and backfilled with argon 3 times. The degassed toluene (10 mL) were added with syringe, the mixture was allowed heated to 70 ℃, the reaction mixture was cooled to room temperature and diluted with ethyl acetate, washed with brine and water, dried over Na_2SO_4, filtered and concentrated. The residue was purified with silica gel chromatography using PE/EA=30:1 as eluent to provide product **N-mIPh-SMe** as yellow solid (140 mg, yield: 41.1%); ^{1}H NMR (400 MHz, $CDCl_3$) δ 7.39 (s, 1H), 7.29 (d, *J* = 8.0 Hz, 2H), 7.27 – 7.25 (m, 1H), 7.06 (d, *J* = 8.4 Hz, 2H), 6.99 (s, 1H), 6.98 (s, 1H), 5.68 (s, 1H), 2.52 (s, 3H). ^{13}C NMR (101 MHz, $CDCl_3$) δ 144.9, 140.0, 130.9, 130.8, 129.6, 129.5, 125.6, 119.9, 116.3, 95.1, 17.6.

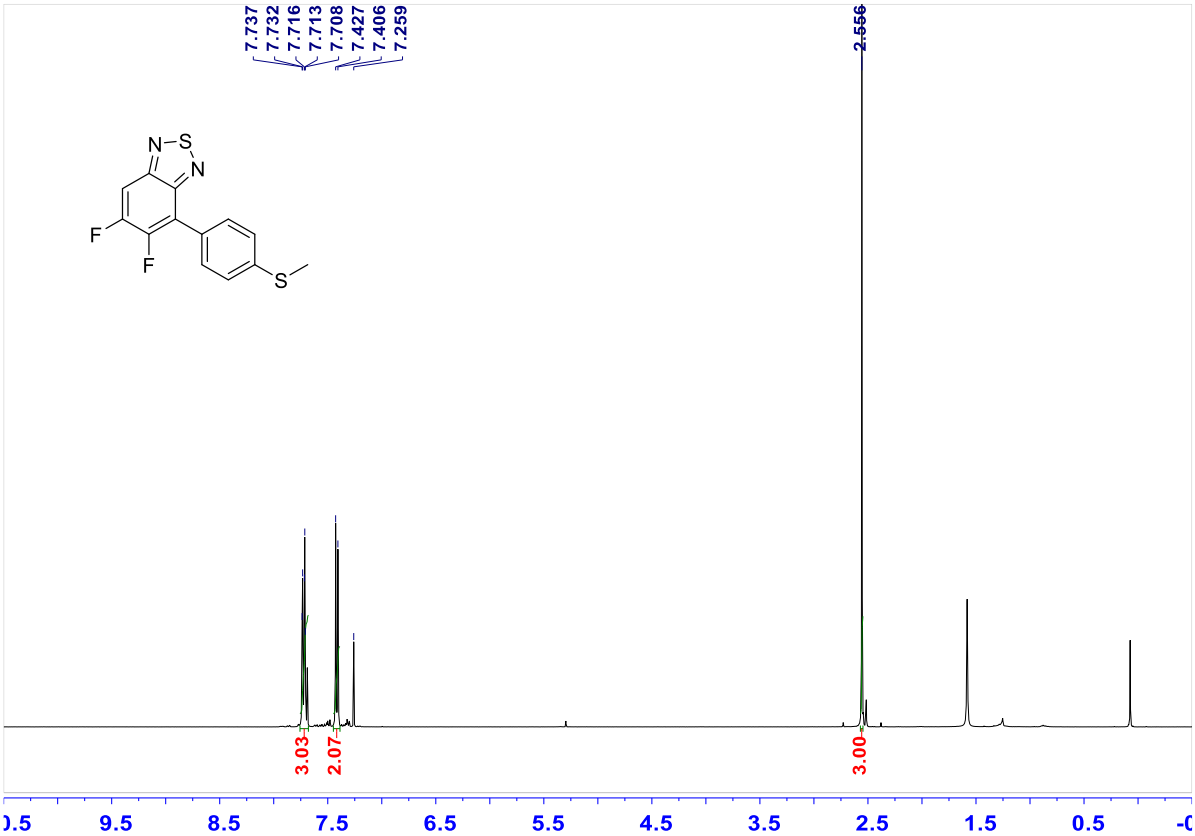

Figure S1. ^{1}H NMR spectrum (400 MHz, $CDCl_3$) of **FBTZ-SMe**

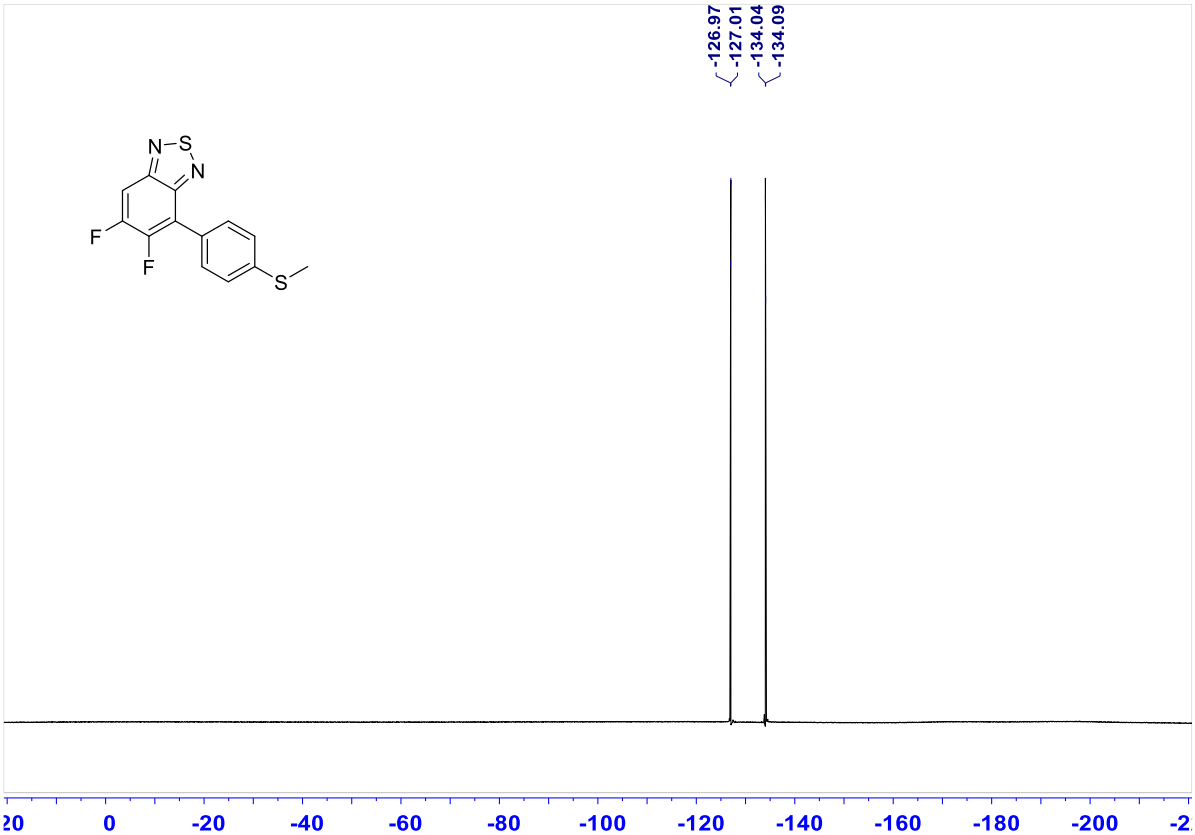

Figure S2. ^{19}F NMR spectrum (376 MHz, $CDCl_3$) of **FBTZ-SMe**

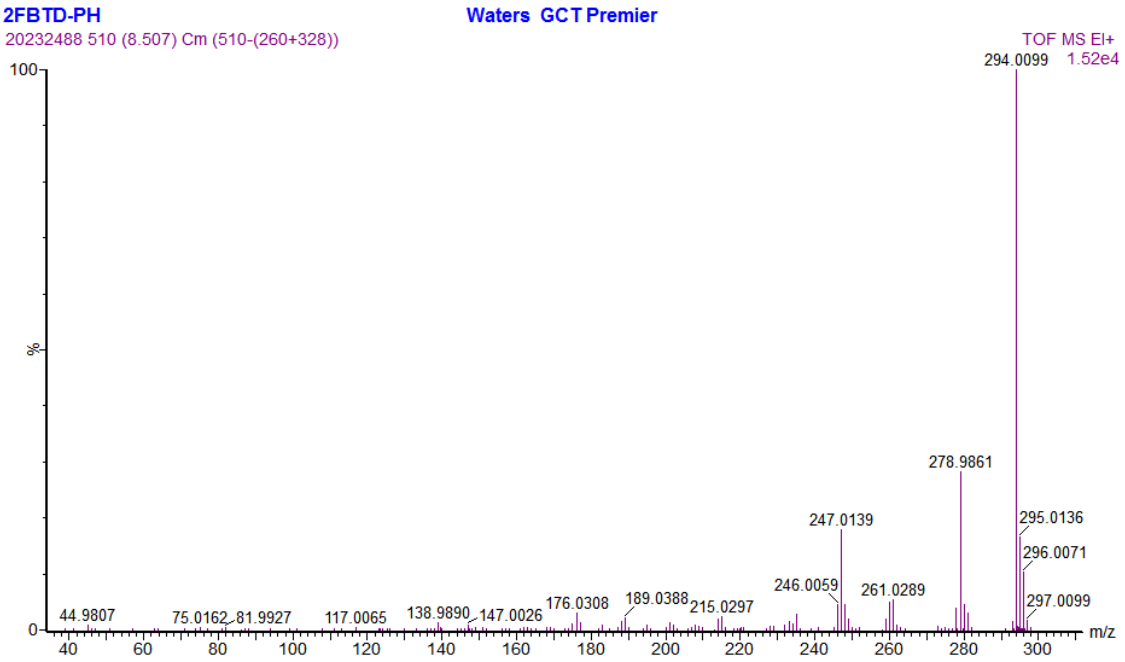

Figure S3. HRMS of **FBTZ-SMe**

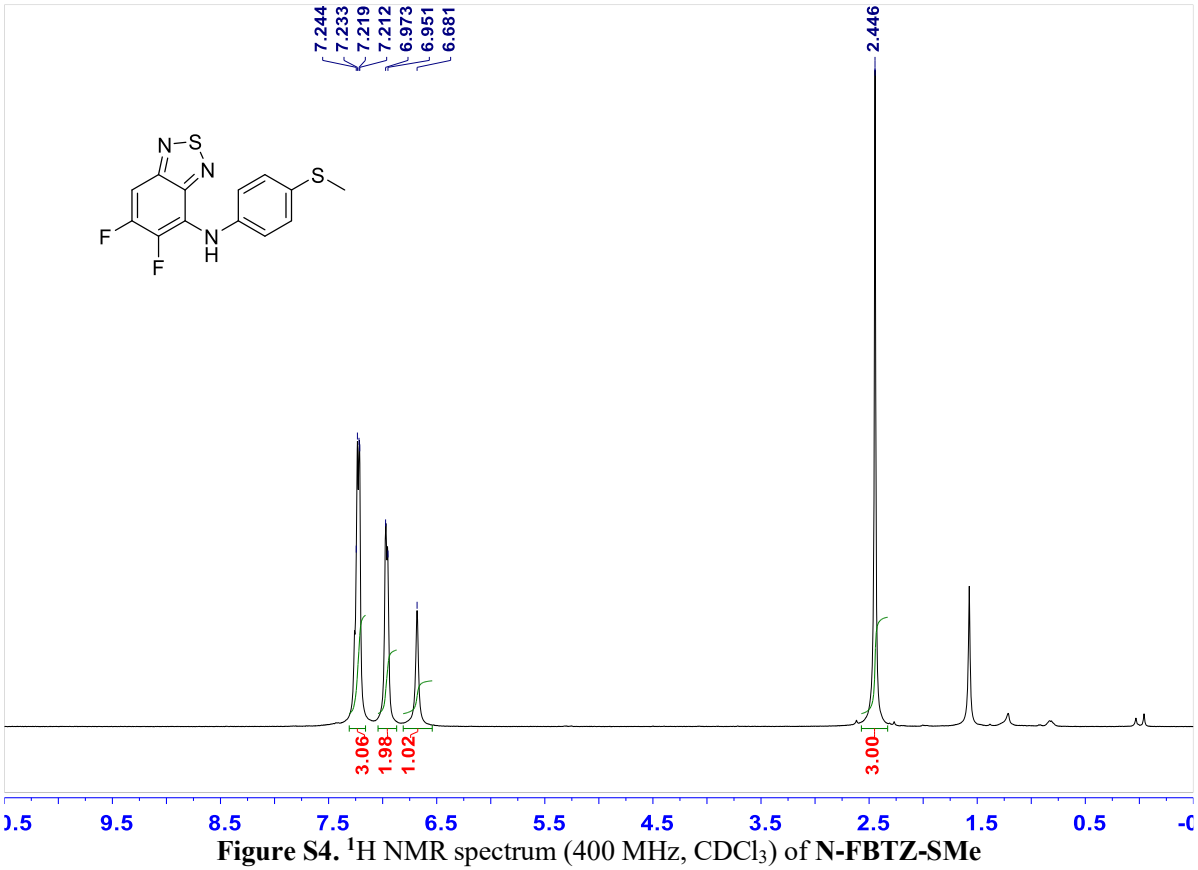

Figure S4. ^{1}H NMR spectrum (400 MHz, $CDCl_3$) of **N-FBTZ-SMe**

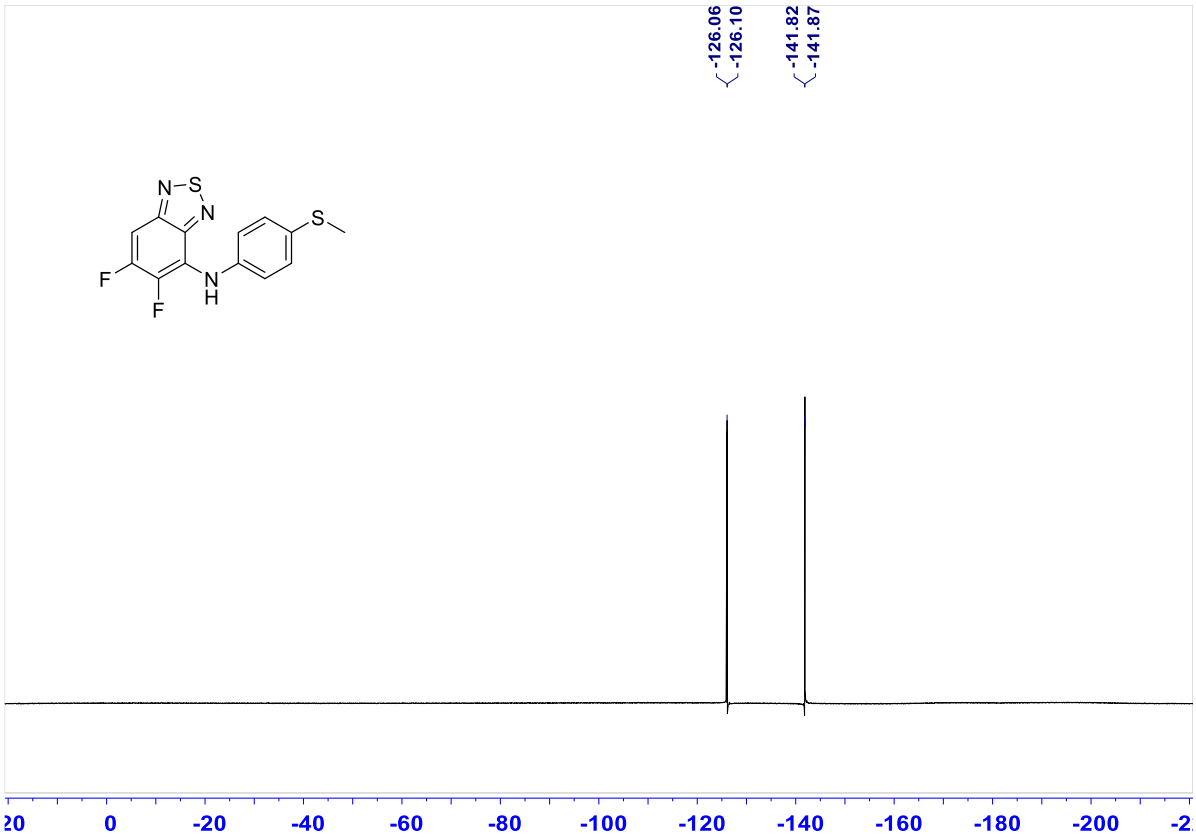

Figure S5. ^{19}F NMR spectrum (376 MHz, $CDCl_3$) of **N-FBTZ-SMe**

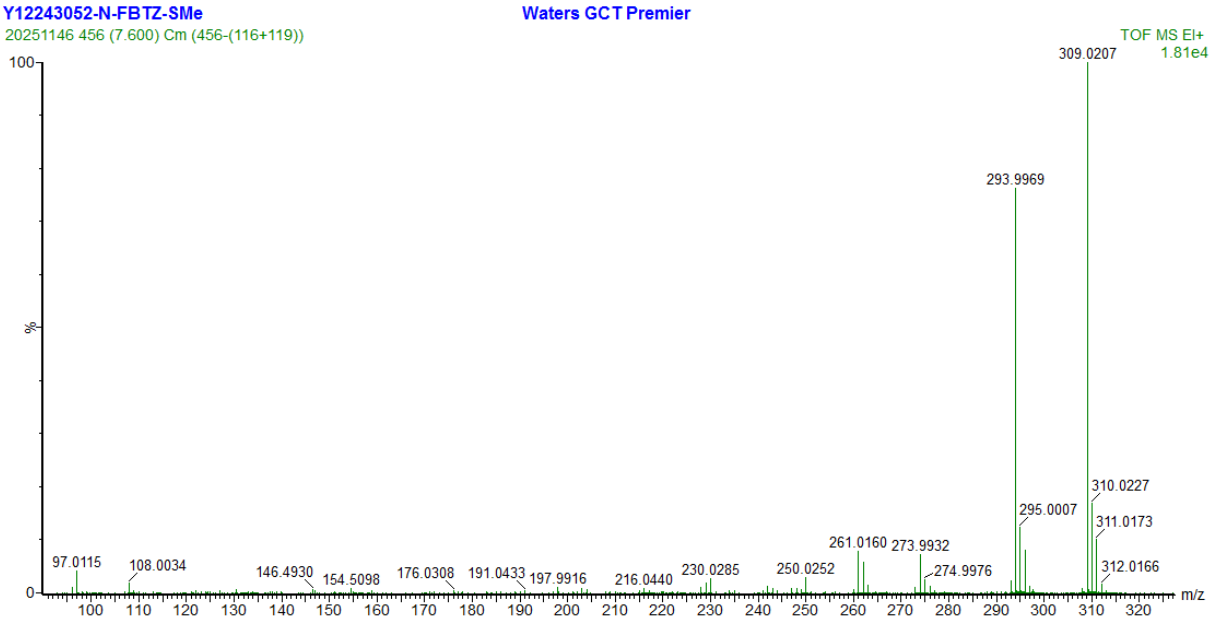

Figure S6. HRMS of **N-FBTZ-SMe**

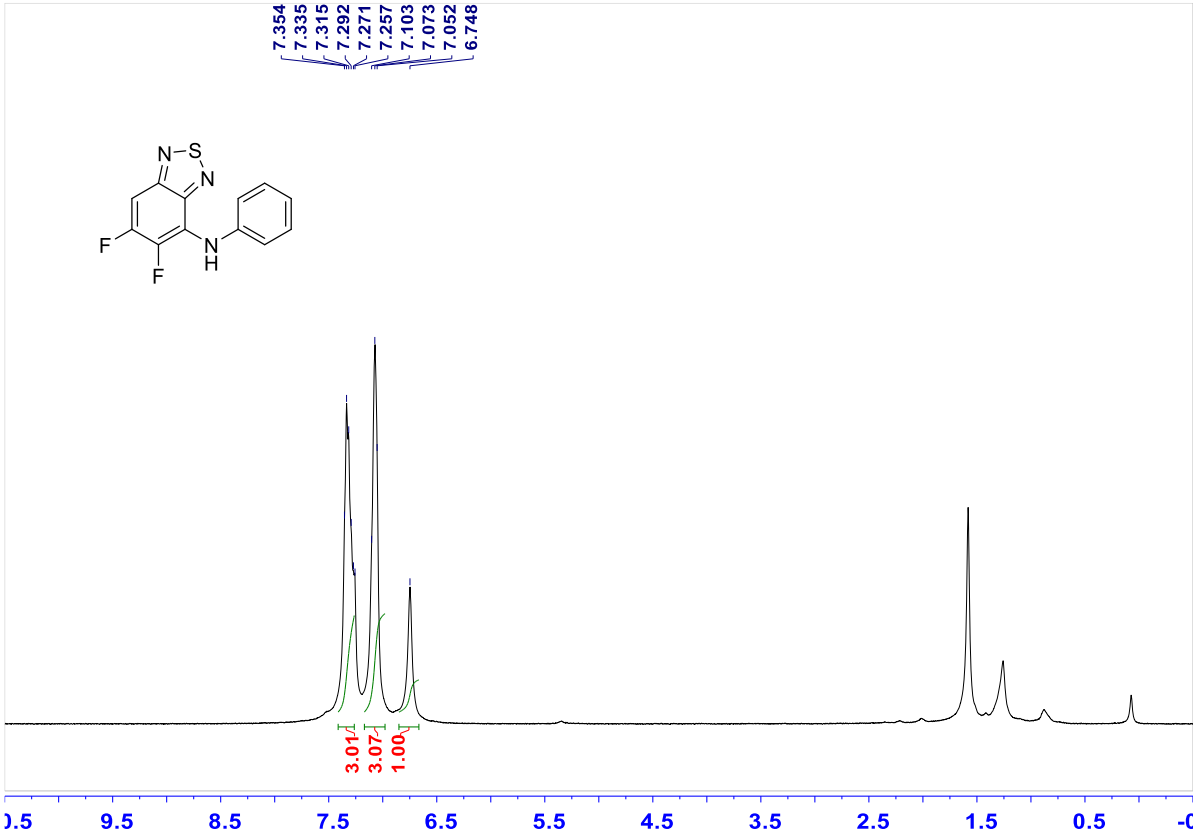

Figure S7. ^{1}H NMR spectrum (400 MHz, $CDCl_3$) of **N-FBTZ**

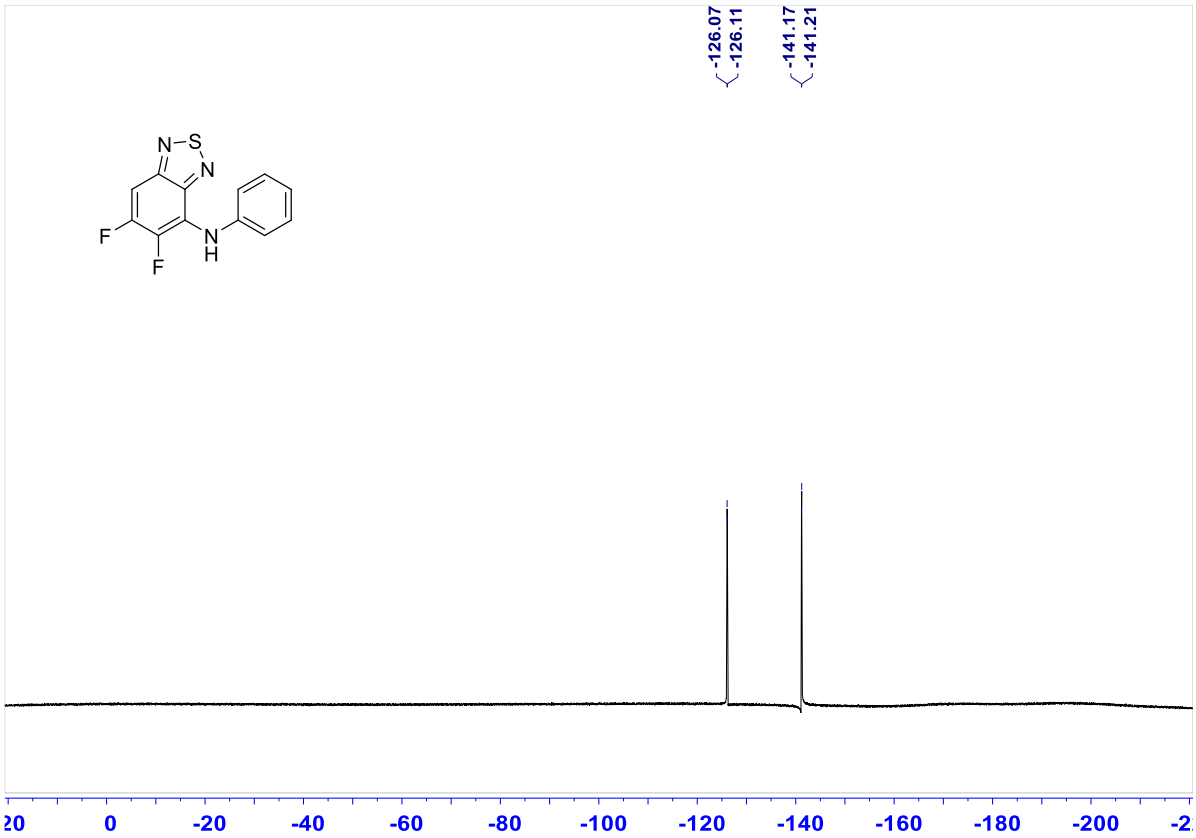

Figure S8. ^{19}F NMR spectrum (376 MHz, $CDCl_3$) of **N-FBTZ**

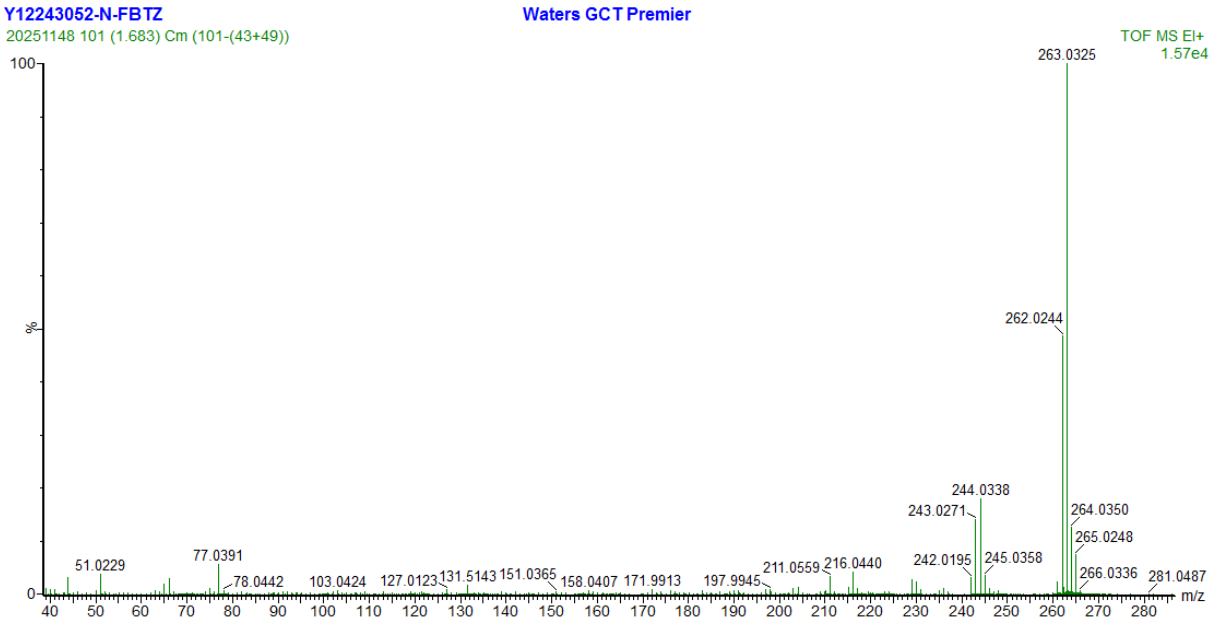

Figure S9. HRMS of **N-FBTZ**

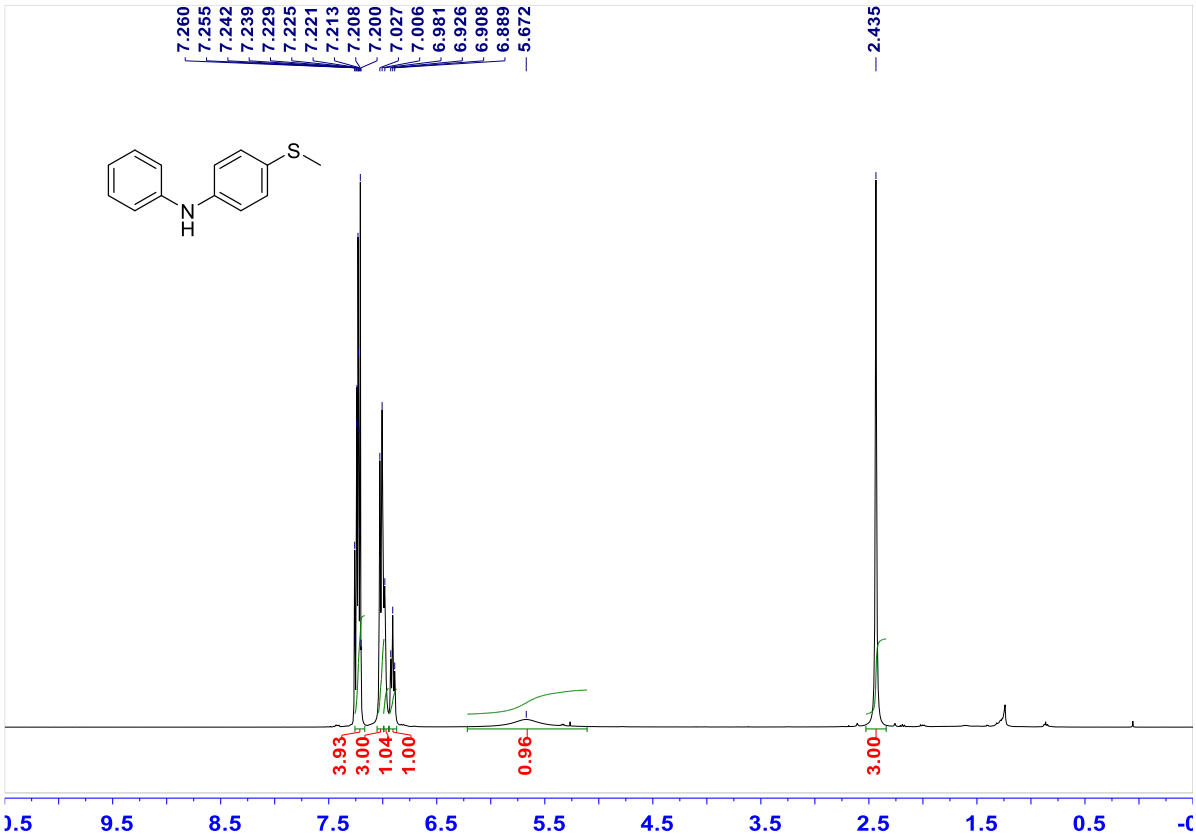

Figure S10. ^{1}H NMR spectrum (400 MHz, $CDCl_3$) of **N-Ph-SMe**

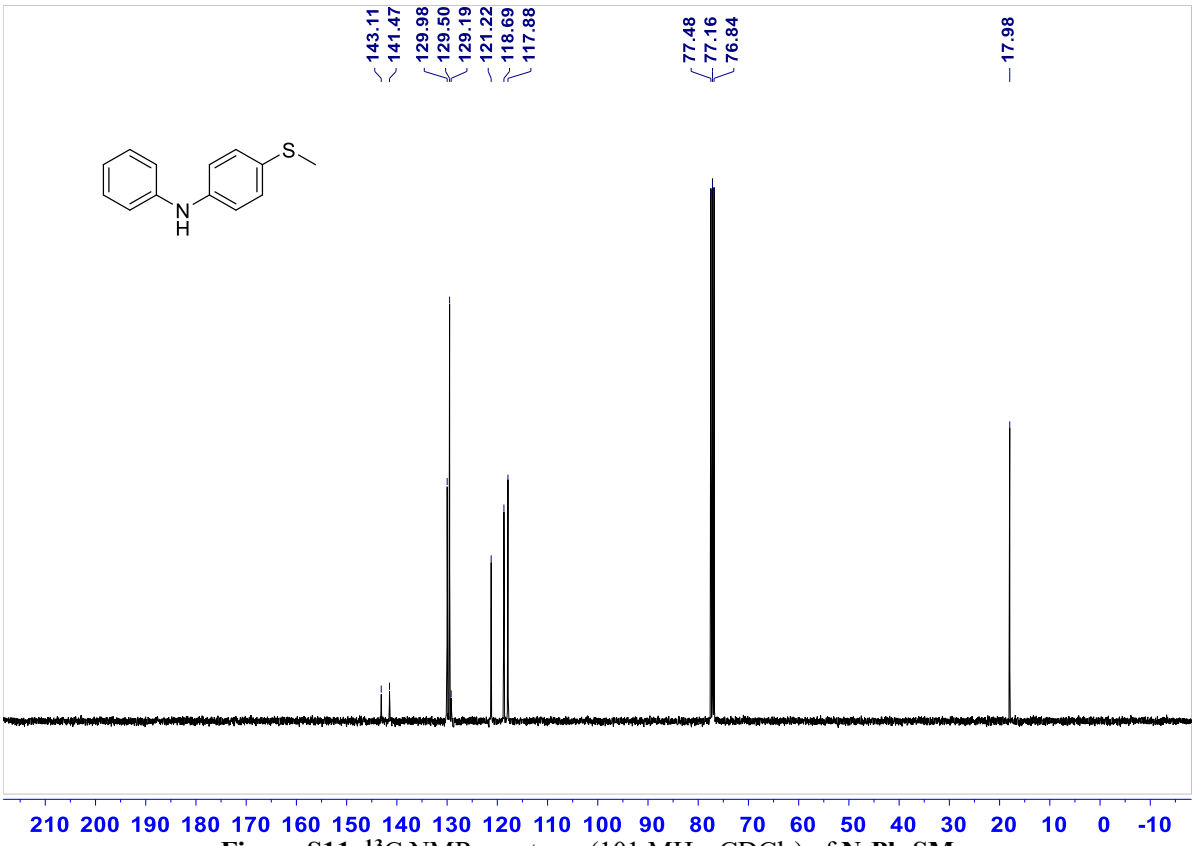

Figure S11. ^{13}C NMR spectrum (101 MHz, $CDCl_3$) of **N-Ph-SMe**

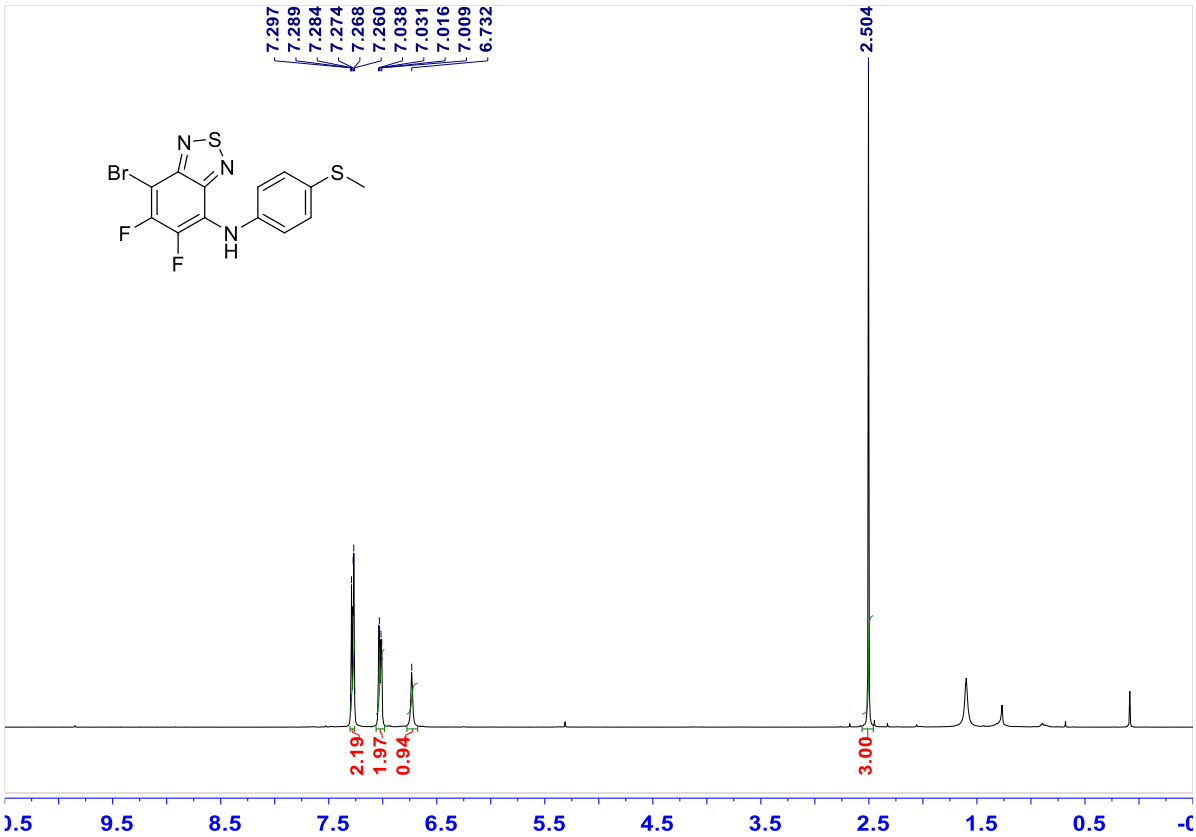

Figure S12. ^{1}H NMR spectrum (400 MHz, $CDCl_3$) of **N-BrFBTZ-SMe**

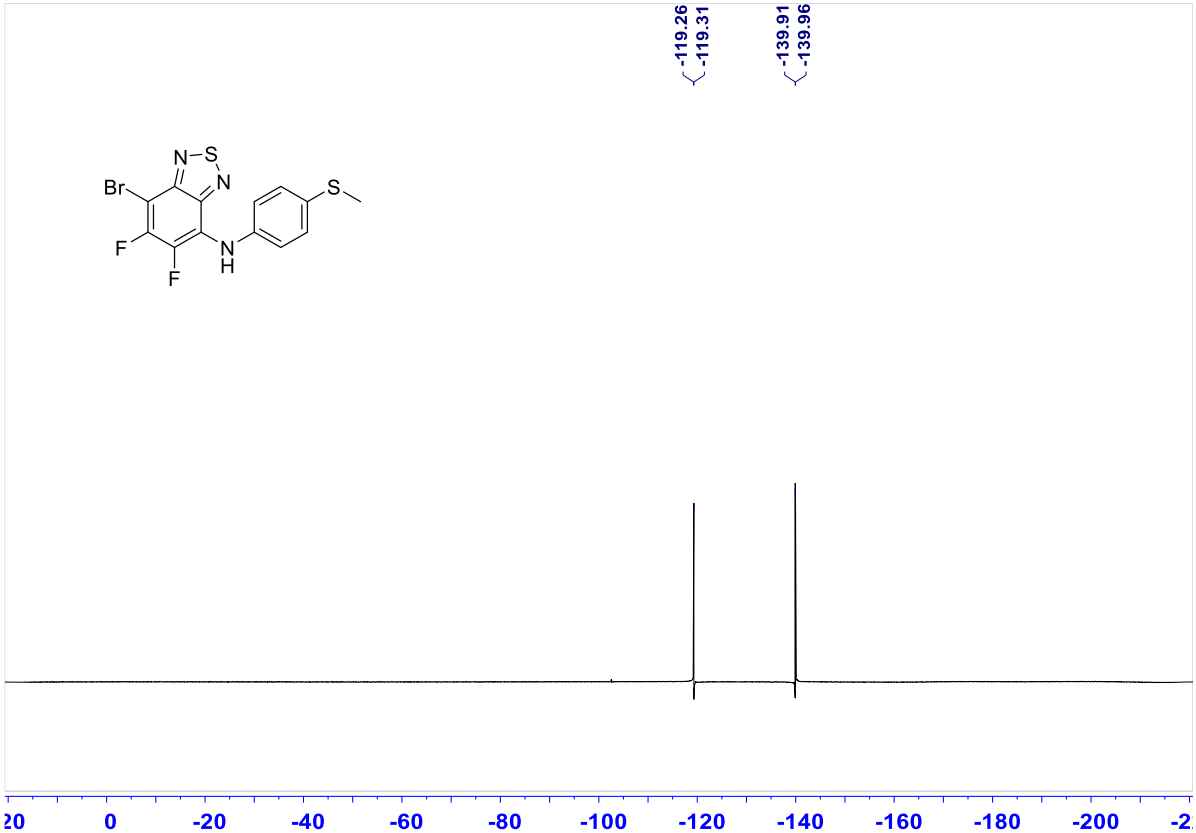

Figure S13. ^{19}F NMR spectrum (376 MHz, $CDCl_3$) of **N-BrFBTZ-SMe**

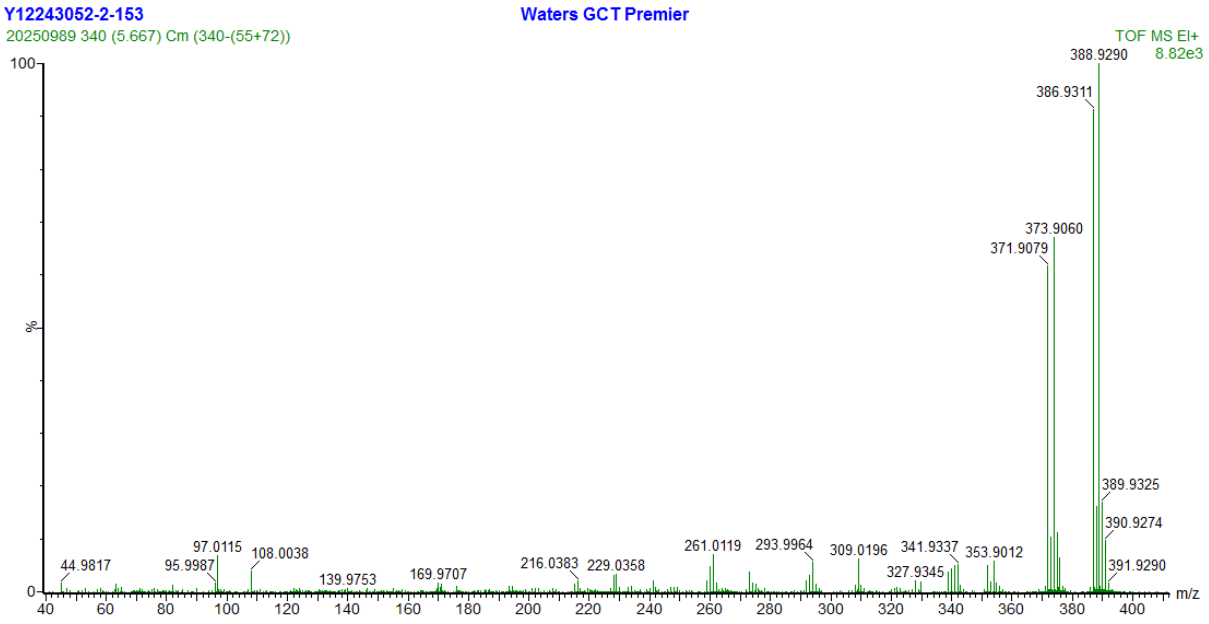

Figure S14. HRMS of **N-BrFBTZ-SMe**

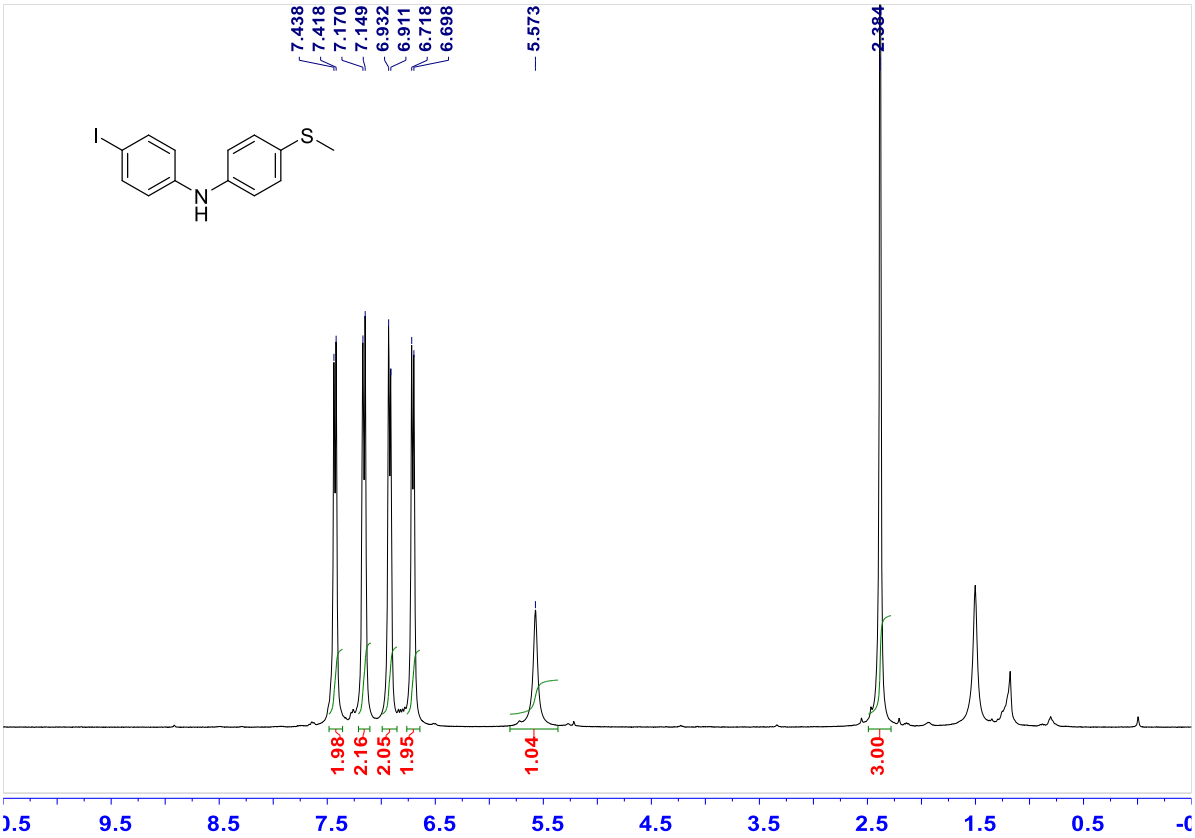

Figure S15. ^{1}H NMR spectrum (400 MHz, $CDCl_3$) of **N-IPh-SMe**

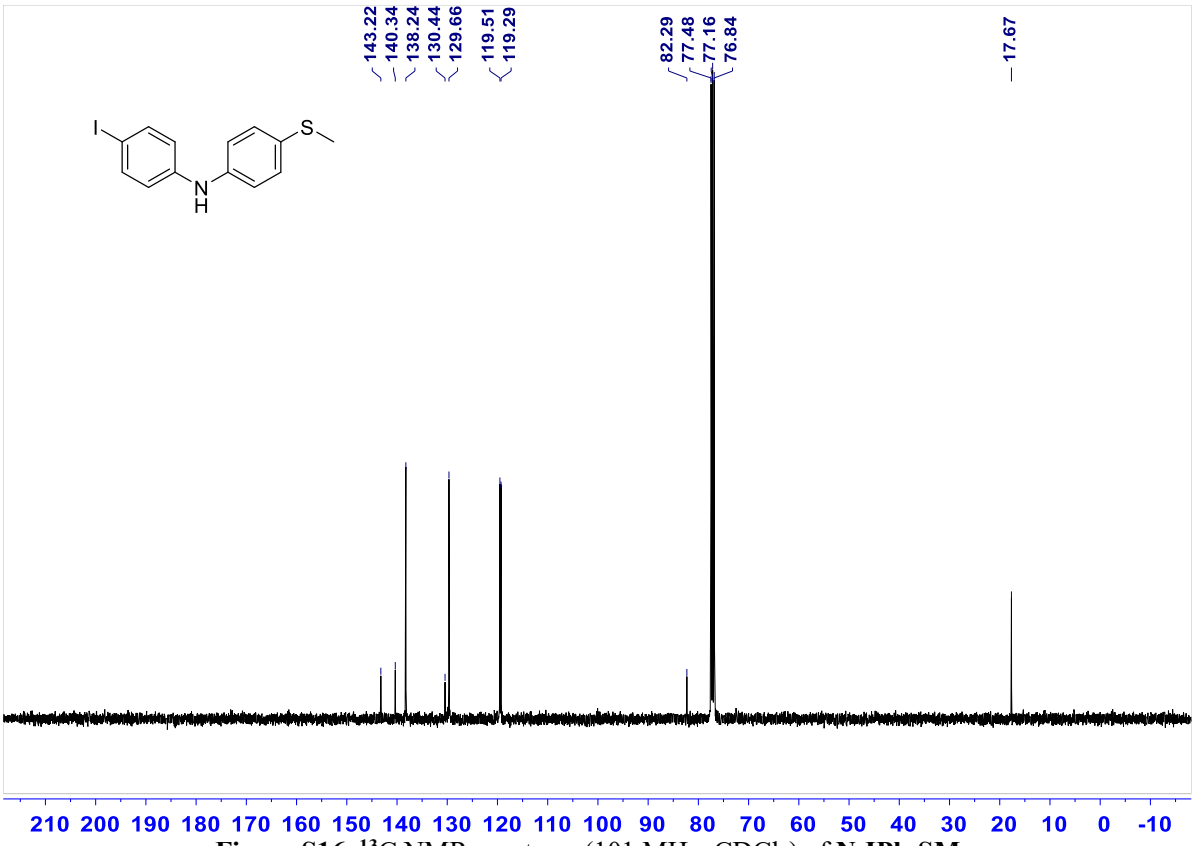

Figure S16. ^{13}C NMR spectrum (101 MHz, $CDCl_3$) of **N-IPh-SMe**

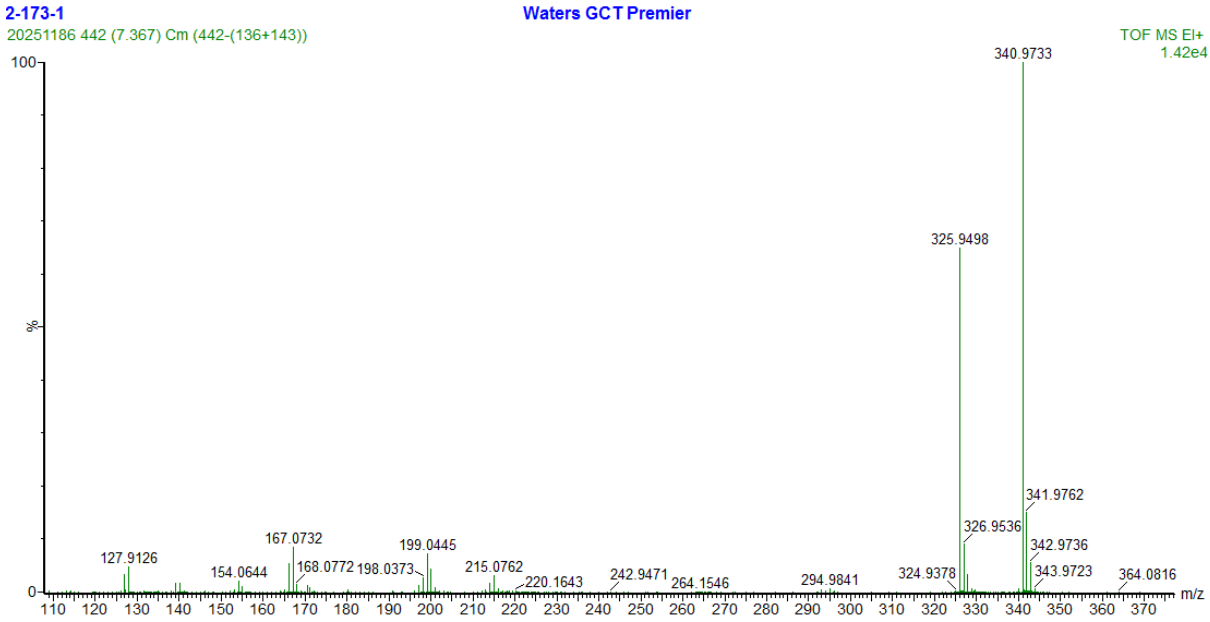

Figure S17. HRMS of **N-IPh-SMe**

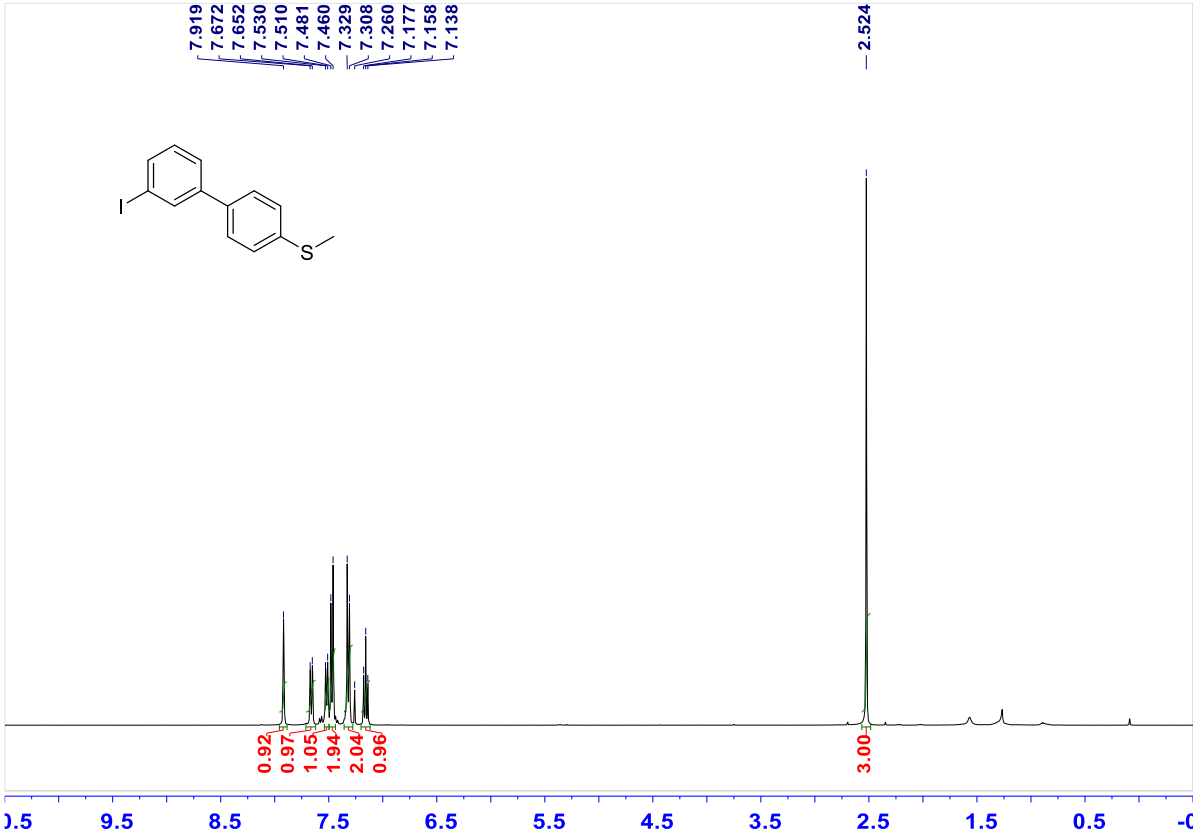

Figure S18. ^{1}H NMR spectrum (400 MHz, $CDCl_3$) of **mIPh-SMe**

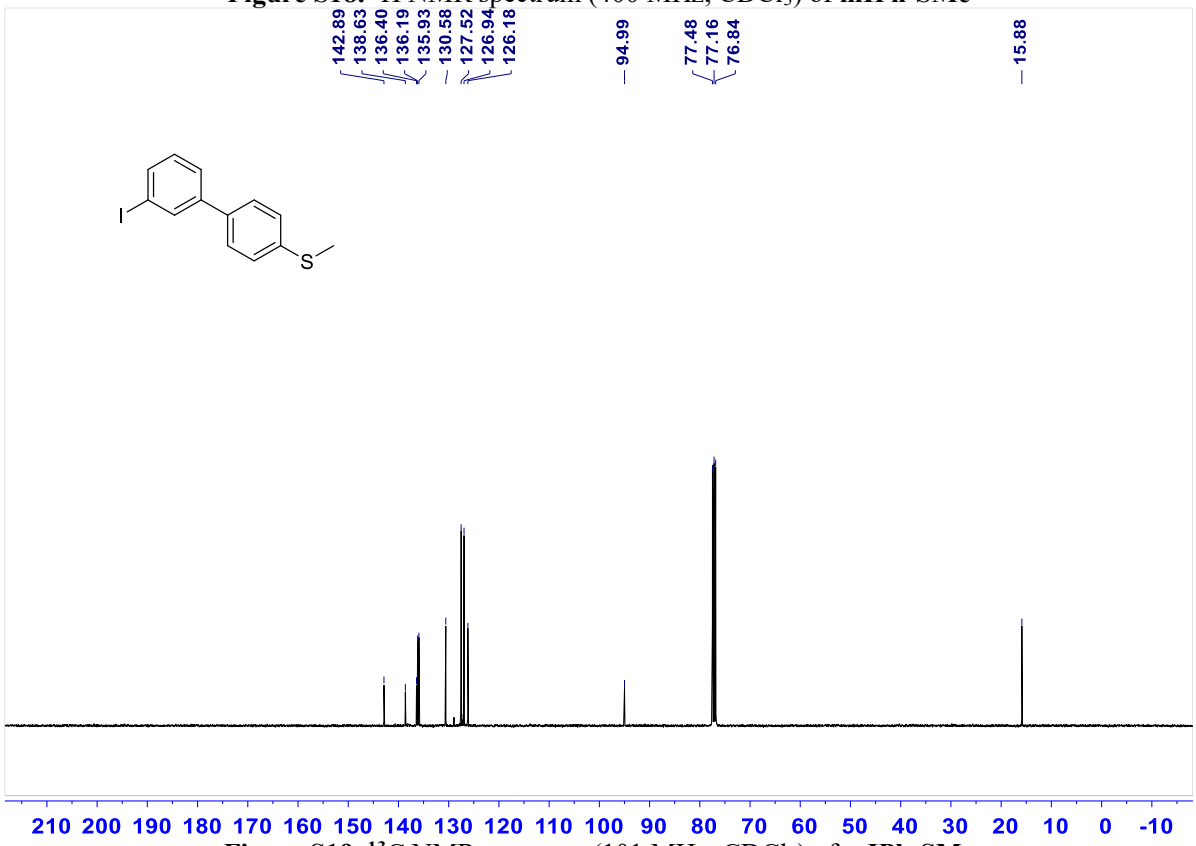

Figure S19. ^{13}C NMR spectrum (101 MHz, $CDCl_3$) of **mIPh-SMe**

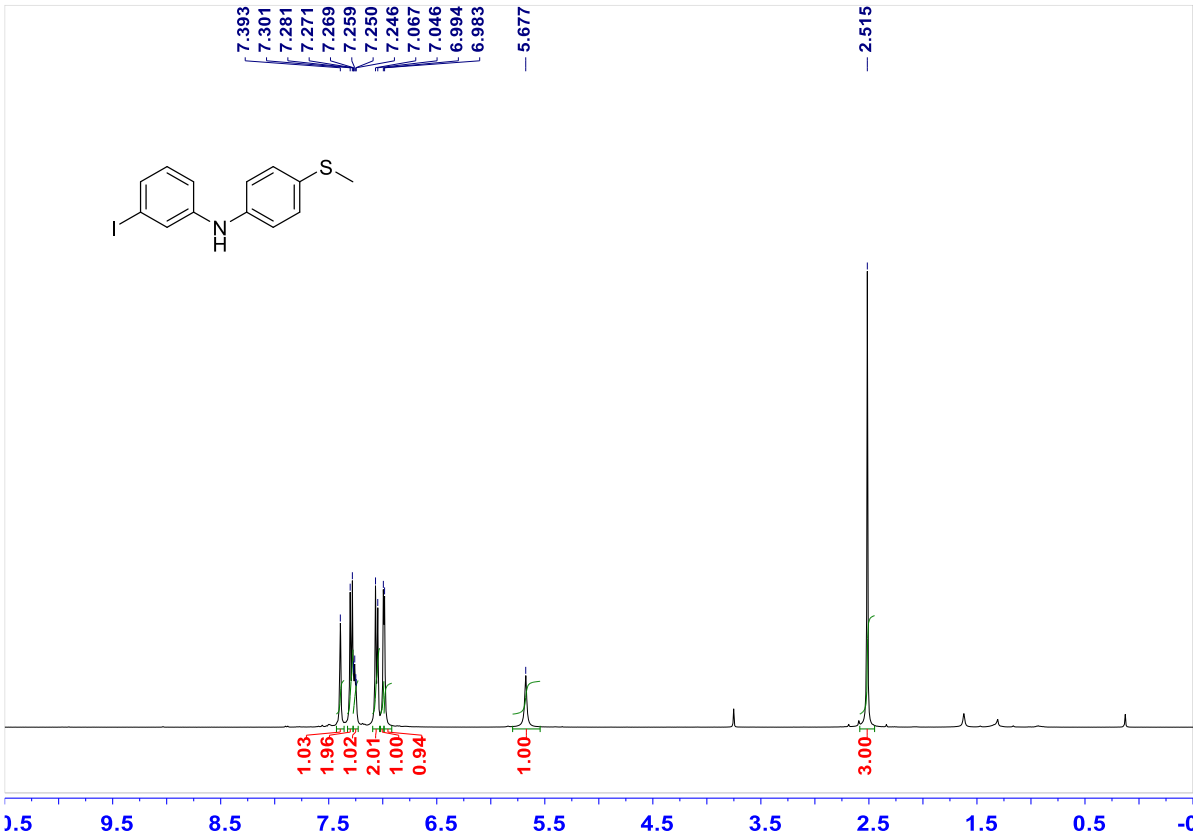

Figure S20. ^{1}H NMR spectrum (400 MHz, $CDCl_3$) of **N-mIPh-SMe**

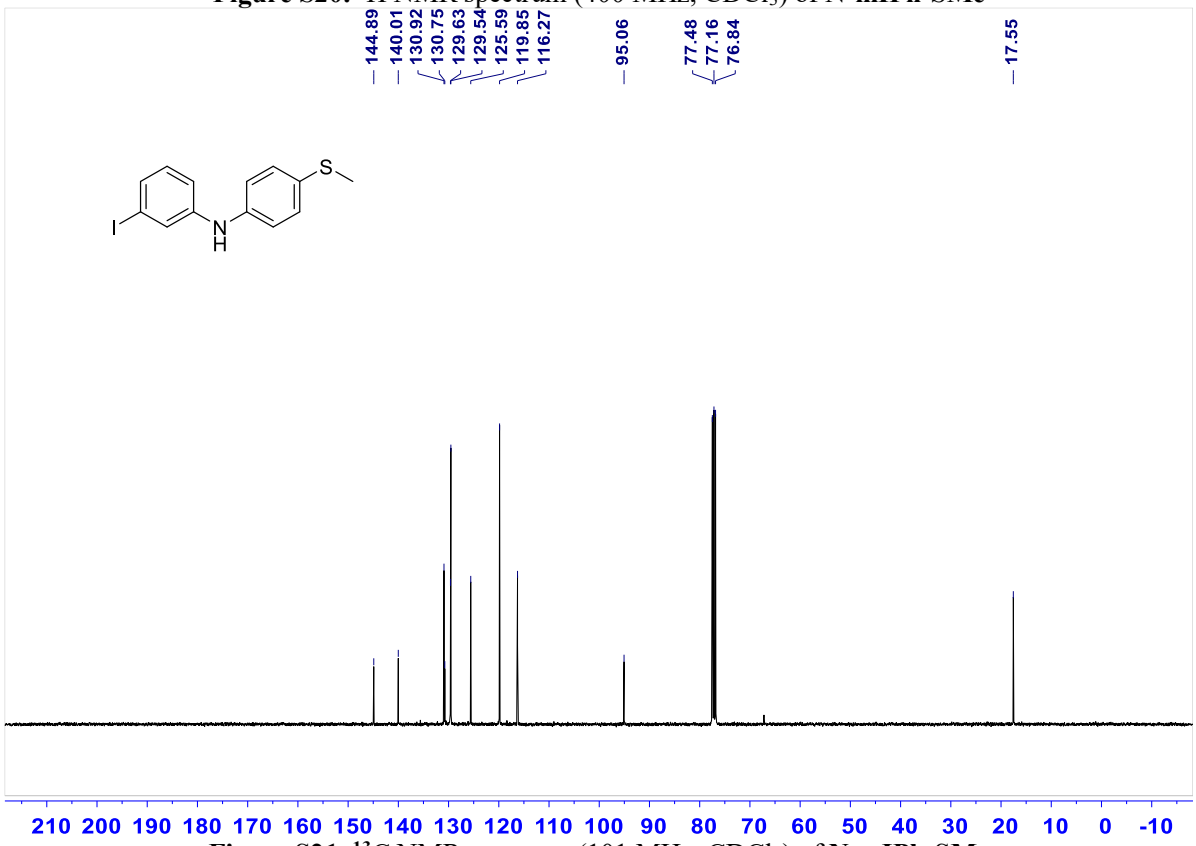

Figure S21. ^{13}C NMR spectrum (101 MHz, $CDCl_3$) of **N-mIPh-SMe**

3. UV-vis and CV

UV–vis absorption spectra of the compounds were collected using a Nicolet CARY 100 spectrophotometer.

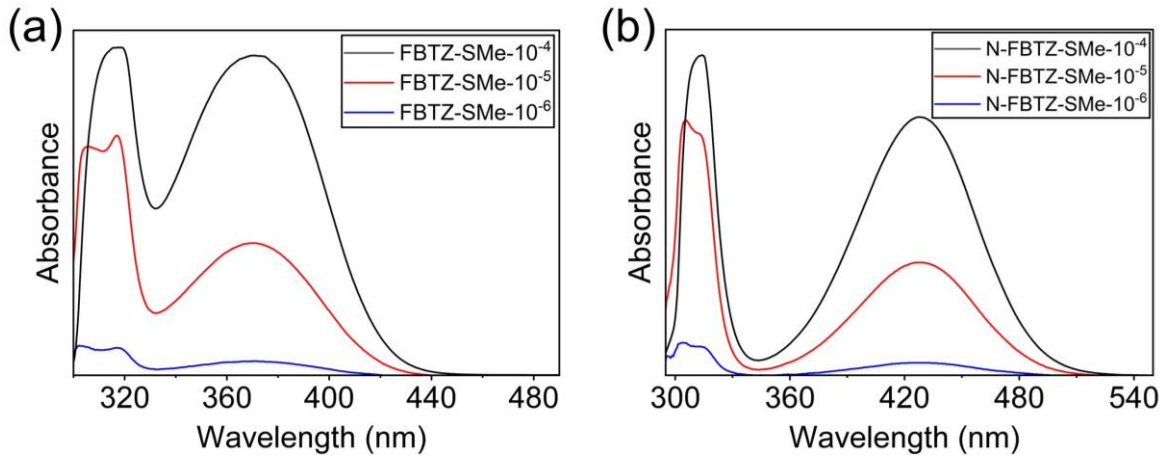

Figure S22. UV-vis absorption spectra of target molecules (10^{-6} to 10^{-4} mol/L in TCB). (a) **FBTZ-SMe**; (b) **N-FBTZ-SMe**.

Cyclic voltammetry (CV) measurements were carried out on a CHI760E electrochemical workstation under a nitrogen atmosphere at room temperature. Sample solutions (0.1 mM in dichloromethane, Bu_4NPF_6 as the supporting electrolyte) were analyzed using a gold working electrode, a platinum wire counter electrode, and an Ag/AgCl (3 M KCl) reference electrode.

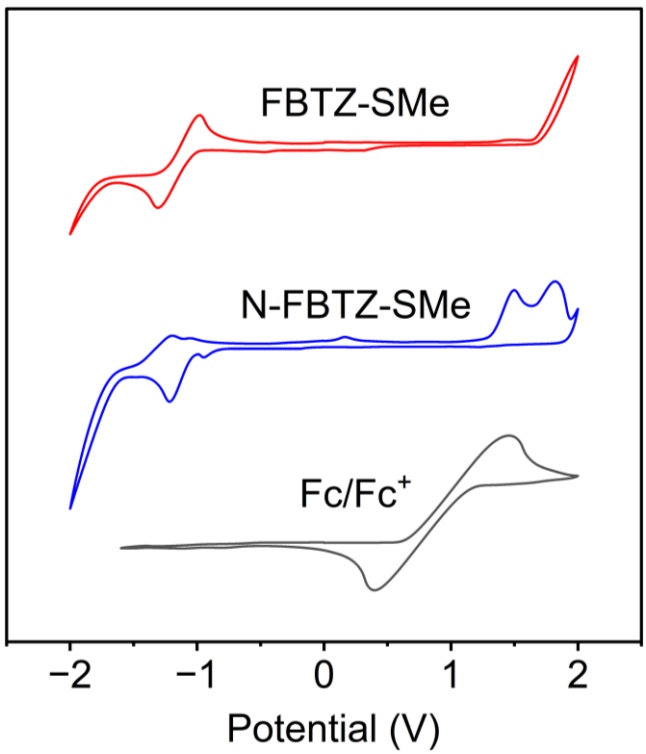

Figure S23. Cyclic voltammograms of FBTZ molecules.

4. Conductance Measurements

In the STM-BJ measurement, the gold tips were fabricated using gold wires (99.99%, 0.25 mm diameter), which were heated to form beads and attached to the piezo. A gold film was evaporated onto a silicon wafer to fabricate the substrate, which was placed beneath the tips. The single-molecule conductance was measured using a custom-built STMBJ setup that has been described.[4-5] In the STMBJ measurement, the gold tip is firstly controlled by a stepper motor to get to the approximate position to contact the substrate, thereafter the tip is controlled by a piezo stack with the approach/retract at the speed of 10 nm s^{-1}. During the measurements, 10 μL of 0.1 mM target molecule in 1,2,4-trichlorobenzene (TCB) was prepared and dropped onto the substrate in situ. As a result, the single-molecule junctions can be established and broken repeatedly. The current was used as the feedback signal to control the movement of the gold tip. During the repeated opening and closing cycles, the conductance versus displacement traces were collected, and the traces from the opening cycles were used to perform further analyses.

To ensure the accuracy of the measurements, pure solvent correction was conducted before the experiments as shown in Figure S24.

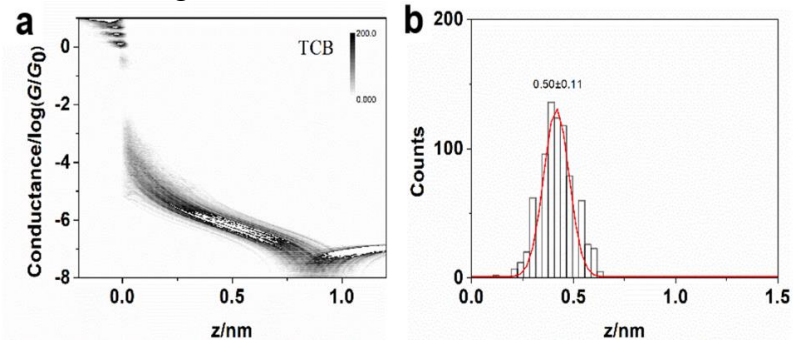

Figure S24. (a) Two-dimensional conductance histogram of blank solvent. (b) Relative displacement distribution. The conductance ranges to determine the relative displacement distribution are from $10^{-0.3}$ ~ $10^{-6.0}$ G_0. No obvious conductance peak signal was found in the blank solvent measurement. The stretching distance is Δz=0.50±0.11 nm (the error is the standard deviation), corresponding to the gold snap-back distance.

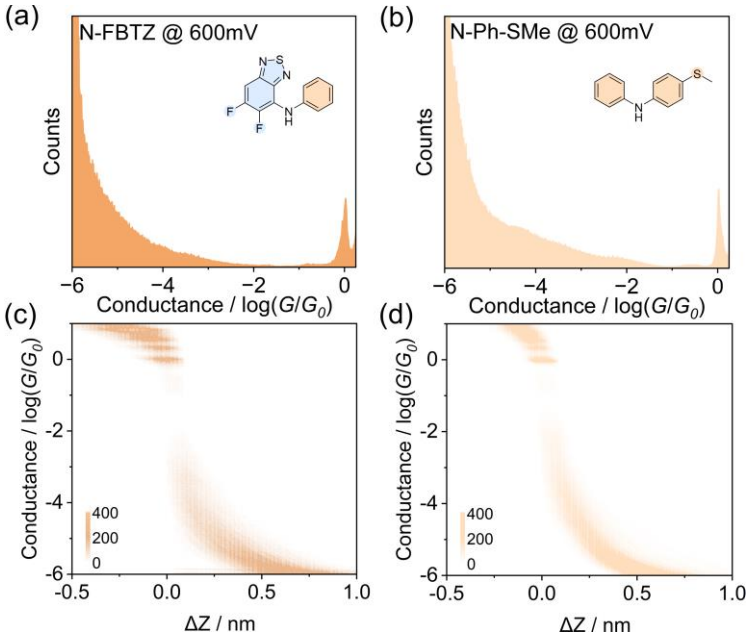

Figure S25. 1D and 2D conductance histograms of **N-FBTZ** and **N-Ph-SMe** at 600 mV. (a,c) **N-FBTZ**; (b,d) **N-Ph-SMe**. The insets show the chemical structures of **N-FBTZ** and **N-Ph-SMe**.

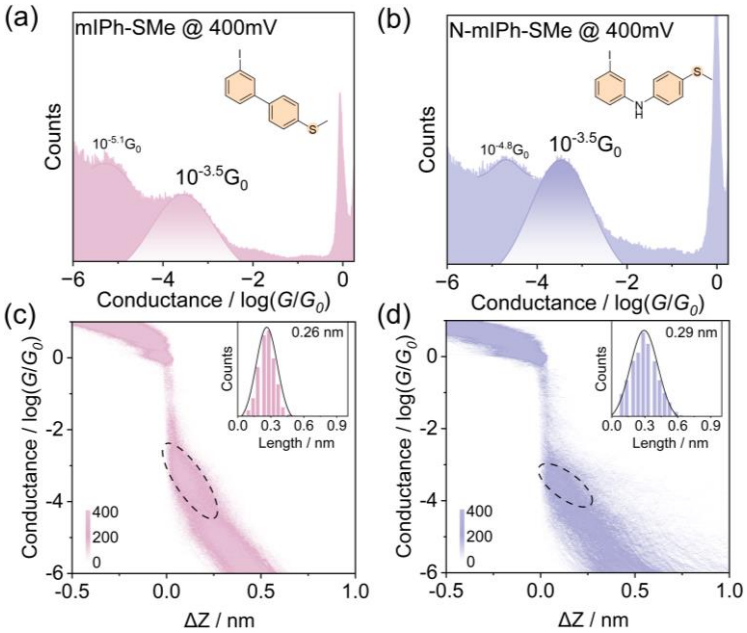

Figure S26. (a,b) 1D conductance histograms of **mIPh-SMe** and **N-mIPh-SMe** at 400 mV. The insets show the chemical structures of **mIPh-SMe** and **N-mIPh-SMe**. (c,d) 2D conductance-displacement histograms of **mIPh-SMe** and **N-mIPh-SMe** at 400 mV. The insets show the plateau-length distributions of **mIPh-SMe** and **N-mIPh-SMe** at 400 mV. The low conductance peak is assigned to Au–I dative-bonded junctions.

The flicker noise spectra were acquired by holding the gold tip in a fixed distance while maintaining molecular junction device. When the corresponding conductance plateau was formed within preset conductance range during the break junction measurement, the bias was hold to produce G–t data which was further transformed into I–t plots. When the I–t plots were recorded, the noise power spectral densities were obtained by calculating the square of the discrete Fourier transform of a conductance. The flicker noise spectrum is a common method in molecular electronics to identify charge transport pathways. A noise power below 1.5 typically indicates that the dominant charge transport mechanism is 'through bond,' while a noise power exceeding 1.5 suggests 'through space' charge transport. Further details on this analysis can be found in previous studies.

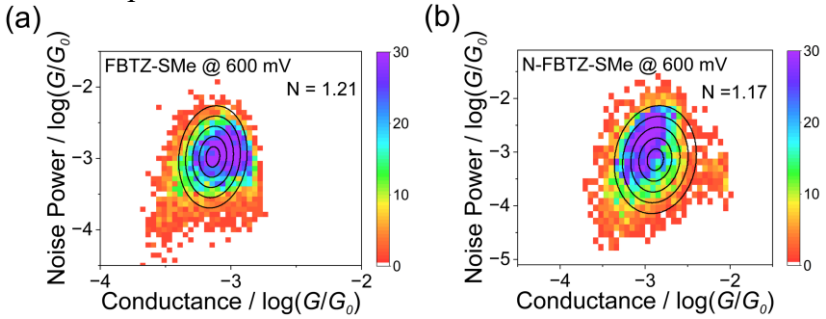

Figure S27. The 2D histograms of the normalized noise power versus average conductance for **FBTZ-SMe** (a) and **N-FBTZ-SMe** (b) at 600 mV.

For I-V measurements, a procedure similar to the flicker noise spectra hovering procedure was performed while the scanning the bias voltage from −1.0 to 1.0 V with a step of 0.003 V to implement current-voltage analysis. The subsequent G-V and FN analysis both derived from corresponding I-V curves. Specifically, the I-V scans were triggered when the conductance fell within the predefined molecular plateau window during junction stretching. For FBTZ-SMe, the conductance window was set to log(G/G0) = −3.7 to −2.9, while for N-FBTZ-SMe, the window was set to log(G/G0) = −3.3 to −2.4. For each molecule, more than 2000 individual I–V traces were collected. These traces were then statistically analyzed and fitted to obtain the representative I–V curves, which were subsequently used to construct the transition voltage spectroscopy (TVS) plots. The data analysis was performed using the XMe open-source code, which can be accessed at the following link: https://github.com/Pilab-XMU/XMe_DataAnalysis. All experimental procedures were carried out at room temperature.

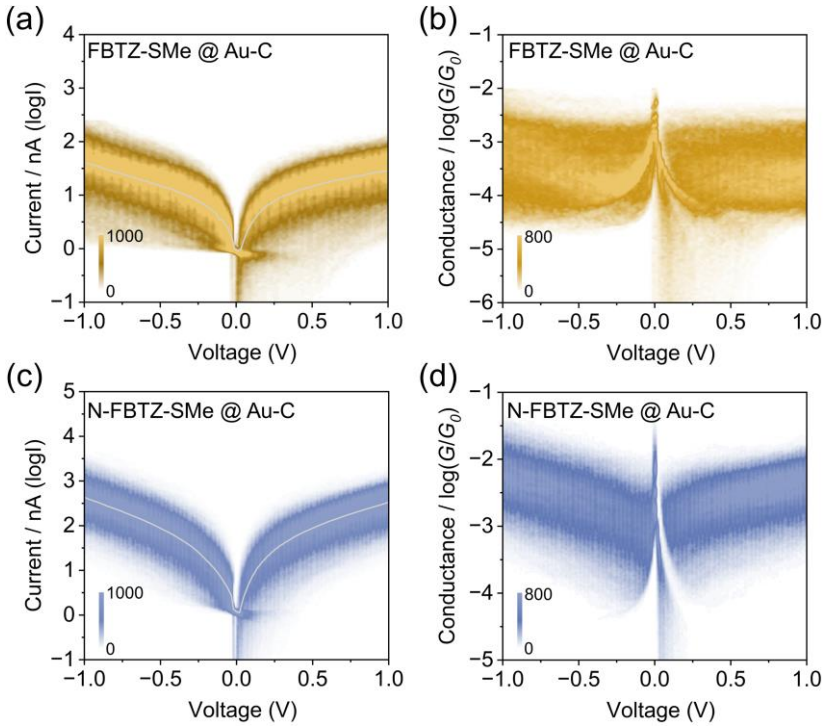

Figure S28. 2D current versus voltage (*I*–*V*) histograms of **FBTZ-SMe** (a) and **N-FBTZ-SMe** (c) junctions with an Au–C bond. 2D conductance versus voltage (*G*–*V*) histograms of **FBTZ-SMe** (b) and **N-FBTZ-SMe** (d) junctions with an Au–C bond.

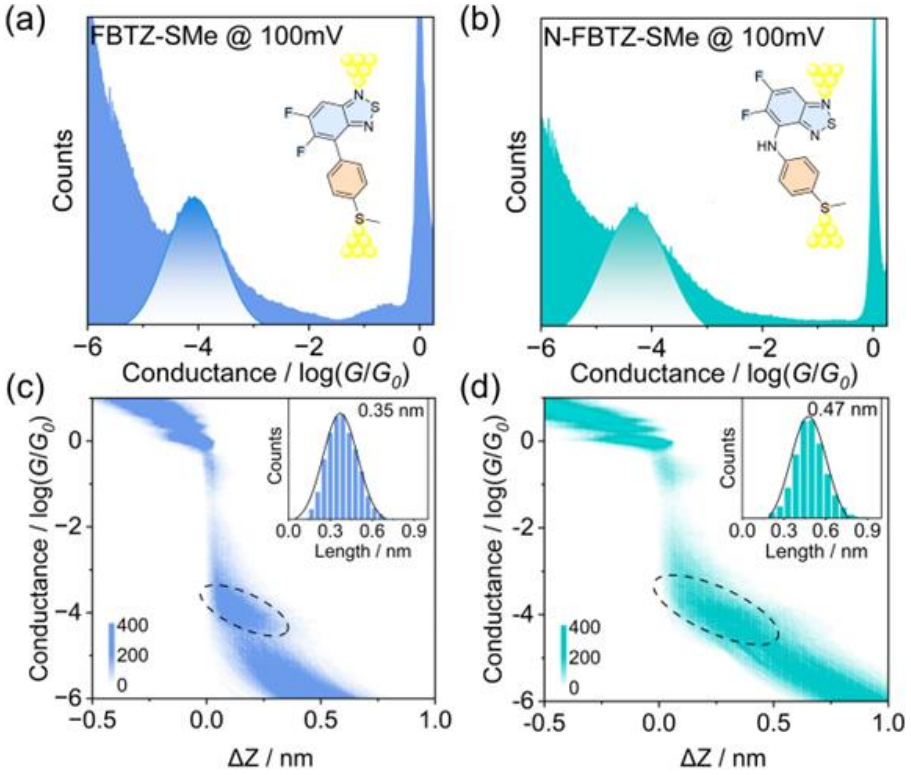

Figure S29. (a-b) 1D conductance histograms of **FBTZ-SMe** and **N-FBTZ-SMe** at 100 mV. The insets show the structures of molecular junctions **FBTZ-SMe** and **N-FBTZ-SMe** at 100 mV. (c-d) 2D conductance-displacement histograms of **FBTZ-SMe** and **N-FBTZ-SMe** at 100 mV. The insets show the plateau-length distributions of **FBTZ-SMe** and **N-FBTZ-SMe** at 100 mV.

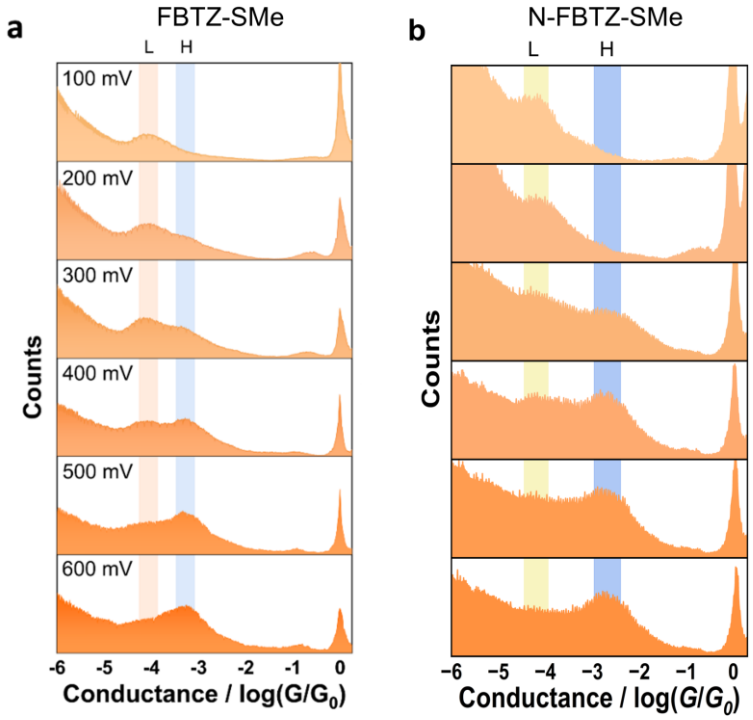

Figure S30. (a,b) 1D conductance histograms of **FBTZ-SMe** and **N-FBTZ-SMe** under the bias voltage ranging from 100-600 mV.

5. DFT calculations

The geometry optimizations were performed using the B3LYP functional and the 6-31G(d,p) basis set with GD3(BJ) dispersion correction, as implemented in the Gaussian 16 software package, and the frequency analysis was performed at the same theoretical level to verify that the stationary points are minimums or transition states. Then, the optimized molecular structures were placed between two gold electrodes to construct the single-molecule junctions. The surface configuration of the gold electrode is constructed as a pyramid. In the initial configuration of the device, the distance between the S atom and the gold atom of the electrode was controlled at about 2.6 Å, the distance gold-carbon bonds was controlled at about 2.1 Å. In configuration optimization, the coordinates of all gold atoms in the electrode are fixed and there are no restrictions on the coordinates of the molecules. The geometry optimization and the transmission spectrum of single-molecule junction were performed using the Quantum ATKQ-2022.03 package, employing the non-equilibrium Green's function (NEGF) formalism. The NEGF-DFT calculations leveraged FHI pseudopotentials and double-zeta polarized atomic orbital basis sets, with the exchange-correlation aspect treated at the PBE generalized gradient approximation (GGA+PBE) level with FHI pseudopotential at single-zeta polarized basis set. The NEGF-DFT self-consistent calculation was deemed converged when each element of the Hamiltonian matrix and density matrix reached a convergence threshold of less than 10^{-5} atomic units. For the computation of the transmission spectra, a 15 × 15 k-point sampling was implemented. The molecular energy spectrum and molecular projected self consistent Hamiltonian (MPSH) spectra of frontier molecular orbital were calculated.

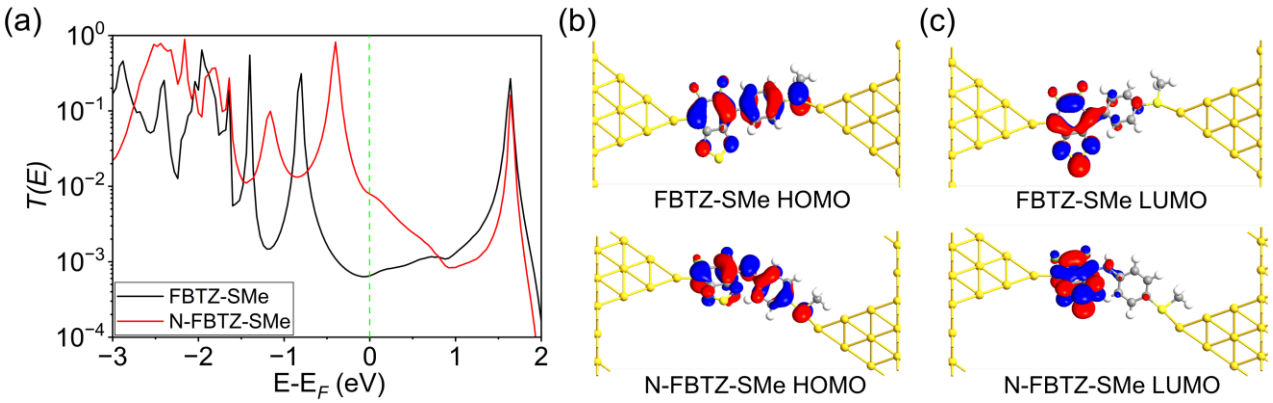

Figure S31. (a) The calculated transmission spectra of **FBTZ-SMe** (black) and **N-FBTZ-SMe** (red) junctions with an Au–C bond. (b,c) The MPSH isosurfaces of Au–C bond for **FBTZ-SMe** (top) and **N-FBTZ-SMe** (bottom). The isovalue is 0.06.

6. Reference

1. Yang, J.; Li, Y.; Zhang, Z.; Li, H. *Chem. Commun.,* **2024***, 60,* 5980−5983.
2. Sakurai, H.; Ritonga, M. T. S.; Shibatani, H.; Hirao, T. *J. Org. Chem.* **2005**, *70*, 2754–2762.
3. Jin, Z.; Lucht, B. L. *J. Am. Chem. Soc.* **2005**, *127*, 5586–5595.
4. Cai, S.; Deng, W.; Huang, F.; Chen, L.; Tang, C.; He, W.; Long, S.; Li, R.; Tan, Z.; Liu, J.; Shi, J.; Liu, Z.; Xiao, Z.; Zhang, D.; Hong, W. *Angew. Chem. Int. Ed*. **2019**, *131,* 3869.
5. Kresse, G.; Furthmüller. *J. Comp. Mater Sci*. **1996**, *6*, 15-50.